SOILS AND FOUNDATIONS Vol. 50, No. 5, 633–644, Oct. 2010
Japanese Geotechnical Society

LARGE-SCALE TRIAXIAL TESTS TO STUDY EFFECTS OF COMPACTION ENERGY AND LARGE CYCLIC LOADING HISTORY ON SHEAR BEHAVIOR OF GRAVEL

SAJJAD MAQBOOL[i] and JUNICHI KOSEKI[ii]

ABSTRACT

This study examines the effects of compaction on peak strength and small strain stiffness of large prismatic specimens of gravel by conducting monotonic and large cyclic loading triaxial compression tests. The specimens were prepared using an automatic compaction system while measuring quantitatively the compaction energy. For the evaluation of small strain stiffness, a static technique using small cyclic vertical loading with local strain measurement and a dynamic technique using P-wave measurement were employed. It was revealed that the peak strength of compacted gravel increased in a non-linear manner with the increase in the compaction energy. On the other hand, the difference between statically and dynamically measured small strain Young's moduli was reduced as a result of increase in the compaction energy. The peak strengths of three almost equally dense specimens were found similar to each other irrespective of the difference in the loading histories with/without large cyclic loading. However, the values of the axial strain at the peak stress state were different among the three specimens, affected by the different loading histories.

Key words: compaction, cyclic loading, gravel, small strain stiffness, strength, triaxial test (**IGC**: D6/D9)

INTRODUCTION

Strength and deformation properties of gravelly soils have been studied for about half a century (Burmister, 1964 among others). Large scale triaxial compression tests on gravelly soils have been conducted to study the properties of fill materials for rockfill dams (e.g., Holtz and Gibbs, 1956; Holtz and Ellis, 1963; Marsal, 1967; Marachi et al., 1969, 1972; Yasuda et al., 1994; Okuyama et al., 2003). In addition, gravelly soils have been investigated in Japan for their use in embankments and backfill of retaining walls to support road and railway structures (e.g., Jiang et al., 1997; Kohata et al., 1999).

Recently, increasing interests in larger and more complex structures of significant importance, such as tracks for bullet trains, high-rise buildings, long-span bridges (e.g., Tatsuoka et al., 1991), have highlighted the need for investigating the behavior of very dense coarse-grained soils, including gravelly fill materials with high compaction. High compaction is also used for the solution of different types of foundation problems in gravelly deposits, in particular where the foundations may be subjected to dynamic and cyclic loadings (Massarsch and Fellenius, 2002).

However, little is known about the effects of high compaction on the properties of gravelly soils, in particular under well-defined compaction conditions in terms of the compaction energy applied. In the present study, therefore, a technique of ''automatic compaction'' is introduced to prepare highly dense specimens of gravel while measuring quantitatively the compaction energy, and the effects of compaction energy on the peak strength and small strain stiffness of the tested material are investigated through a series of triaxial compression tests. In addition, possible effects of large-amplitude cyclic loading on the above properties are also studied, which would contribute towards establishing a rational design method against high seismic loads (Koseki et al., 2007).

It is to be noted that, under working loads, the strain levels within highly dense deposits as well as in well-designed geotechnical structures are relatively small (Tatsuoka and Kohata, 1995). In soil mechanics, it is normally assumed that the ground material is a continuum, and that the behavior is linear and recoverable within a very small strain range i.e., lesser than 10^{-3}% (Tatsuoka and Shibuya, 1992). For the measurement of this ''elastic'' strain range, the experimental devices have to be very precise and accurate.

In the present study, very small vertical unloading/reloading cycles were applied at some stress levels during loading on each gravel specimen, and strains were measured locally using local deformation trans-

[i] Associate Professor, Department of Transportation Engineering and Management, University of Engineering and Technology, Lahore, Pakistan (drsajjadmaqbool@gmail.com).
[ii] Professor, Institute of Industrial Science, The University of Tokyo, Japan.
The manuscript for this paper was received for review on January 15, 2009; approved on May 19, 2010.
Written discussions on this paper should be submitted before May 1, 2011 to the Japanese Geotechnical Society, 4-38-2, Sengoku, Bunkyo-ku, Tokyo 112-0011, Japan. Upon request the closing date may be extended one month.

ducers (LDTs, Goto et al., 1991) within a very small strain range at the specimen sides. This method is herein termed as ''static''. On the same gravel specimen, the velocity of vertically transmitting compression waves (P-waves) was evaluated by triggering with a pulse wave at some stress levels. This method is herein termed as ''dynamic''.

This paper identifies at first the apparatus, measurement techniques, testing material and testing program, followed by discussion on the rationale for the automatic compaction technique in detail. Next we discuss the results of the monotonic and large cyclic loading triaxial compression tests, focusing on the effects of compaction energy on the peak strength and dilatancy properties. Lastly we discuss the effect of compaction energy on small strain stiffnesses obtained by the static and dynamic methods.

APPARATUS, MATERIAL AND TESTING PROGRAM

A large-scale triaxial apparatus (AnhDan et al., 2006a) was employed to conduct triaxial compression tests on compacted gravel specimens. The apparatus consists of a triaxial cell, an axial loading device, and a cell pressure-control device. The axial loading device employs an electro-hydraulic actuator having a capacity of 490 kN and the zero-balance system (Hayano et al., 1999).

For these tests, axial strain (ε_1) was measured by three pairs of vertical local deformation transducers (V-LDTs). Lateral strains in two directions (ε_3) were measured by another three pairs of horizontal local deformation transducers (H-LDTs) and two pairs of cantilever local deformation transducers (C-LDTs, AnhDan et al., 2006b). The directions of ε_1 and ε_3 and the test specimen after setting all LDTs are shown in Photo 1. The schematic diagram showing the location of all LDTs over the specimen is shown in Fig. 1. The mean of data measured with two or three pairs of LDTs was used for each direction of local strain measurement for the analysis of test results.

The testing material was Chiba gravel, used as a fill material in Japan. The grains are in general hard and angular, consisting of well-graded crushed sandstones having $U_c = 30$ and $G_s = 2.71$ (Maqbool, 2005). This material can be categorized into well-graded sandy gravel. Its grain size distribution curves measured before and after heavy compaction for specimen preparation are shown in Fig. 2. The effect of particle crushing due to heavy compaction on the grain size distribution was found to be insignificant. Rather, the content of finer particles having a grain size of about 5 mm or less decreased slightly by the compaction, due possibly to the effect of particle aggregation due to heavy compaction that was not fully recovered during the sieving process.

The friction between the specimen and top cap as well as between the specimen and pedestal was reduced by applying lubrication layers. The lubrication layer comprised 0.8 mm thick rubber membrane and 30-μm thick grease, based on the recommended measure of AnhDan et al. (2006a). No correction for the effects of membrane force was made in the data analysis.

The testing program is summarized in Table 1. For

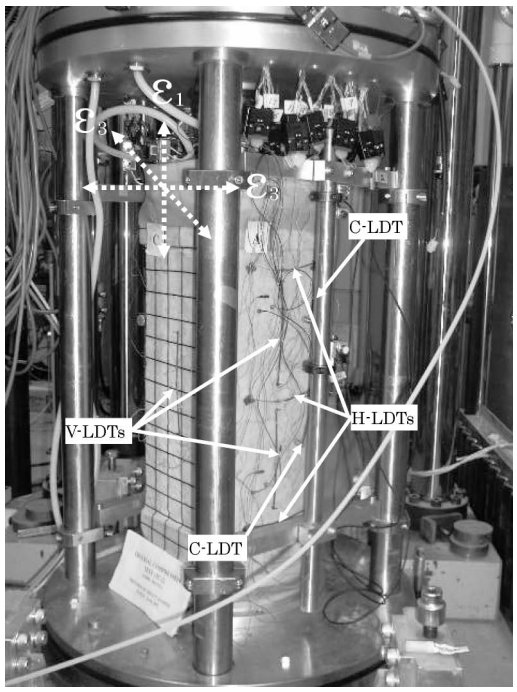

Photo 1. Prismatic specimen after setting all types of LDTs

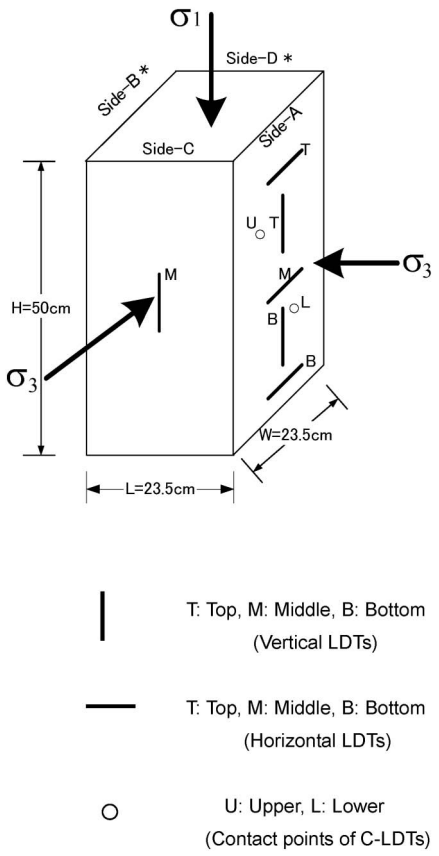

Fig. 1. Positioning of LDTs on triaxial compression test specimen

monotonically loaded tests, after compaction without saturating the specimens, they were first subjected to isotropic compression from a stress state of 49 kPa up to 98 kPa. They were then subjected to isotropic unloading from a stress state of 98 kPa down to 49 kPa. During these isotropic compression and unloading stages, small cyclic vertical loading at several stress levels was applied to evaluate the small strain stiffness. As a result, no significant difference in the small strain Young's moduli measured at the same stress state during the two stages was observed. Then, the specimens were subjected to isotropic re-compression from stress level of 49 kPa to 98 kPa without applying any small cycles of loading. These steps were followed by drained triaxial compression in the vertical direction at $\sigma_3 = 98$ kPa as shown in Fig. 3. At various stress states during otherwise monotonic shearing, in addition to the dynamic measurement, small amplitude unload/reload cycles were applied to evaluate the small strain stiffnesses.

For the large cyclic loading tests, the stress paths as shown in Fig. 4 are followed. The details of the large cyclic loading condition will be described later.

Throughout all the tests, the backpressure was set equal to the atmospheric pressure.

Development of a Compaction Technique and Preparation of Dense Gravel Specimens

In the previous studies, several compaction techniques like vibration for specific time (Dong and Nakamura, 1997), manual compaction (AnhDan and Koseki, 2004) and manual compaction using wooden hammer (Balakrishnaiyer et al., 1998) have been employed. None of these were, however, capable of measuring the compaction energy. These aimed at achieving only the desired

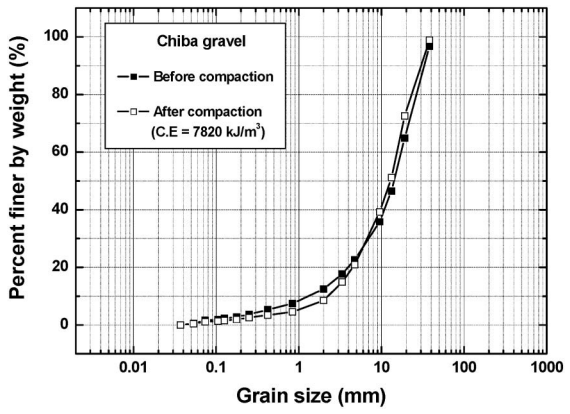

Fig. 2. Gradation curves of tested material (before and after compaction)

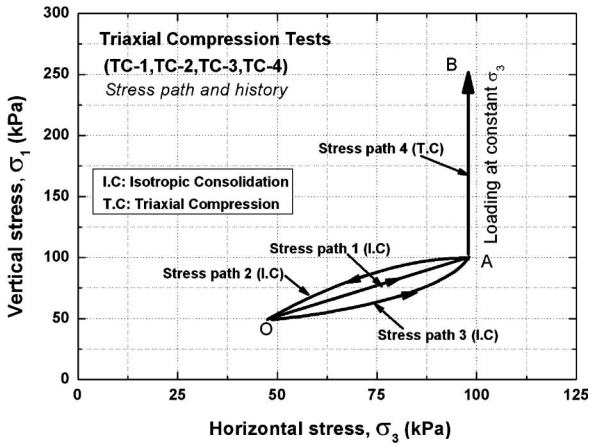

Fig. 3. Stress path in monotonic triaxial compression tests

Table 1. Stress paths followed during monotonic and large cyclic triaxial compression tests

Testing condition	Test code	Loading control	Stress path
Triaxial compression	TC-1 TC-2 TC-3 TC-4	Strain control	I.C. = 49 − 98 − 49 − 98 (kPa)
		Strain control	T.C. at $\sigma_3 = 98$ kPa
Triaxial compression	TC-5	Strain control	I.C. = 49 − 98 − 49 − 98 (kPa)
		Strain control	T.C. with $\sigma_1 = 98 - 539 - 147 - 343$ (kPa), at $\sigma_3 = 98$ kPa
		Stress control	100 L.C. with amp. of 400 kPa, N.A. at $\sigma_1 = 343$ kPa, frequency = 0.00104 Hz and $\sigma_3 = 98$ kPa
		Strain control	T.C. at $\sigma_3 = 98$ kPa
Triaxial compression	TC-6	Strain control	I.C. = 49 − 98 − 49 − 98 (kPa)
		Strain control	T.C. with $\sigma_1 = 98 - 441 - 147 - 441 - 294$ (kPa) at $\sigma_3 = 98$ kPa
		Stress control	100 L.C. with amp. of 300 kPa, N.A. at $\sigma_1 = 294$ kPa, frequency = 0.00104 Hz and $\sigma_3 = 98$ kPa
		Strain control	T.C. at $\sigma_3 = 98$ kPa

I.C.: Isotropic compression
T.C.: Triaxial compression (monotonic loading under otherwise mentioned)
L.C.: Large cycles of loading
N.A.: Neutral axis
amp.: Double amplitude

dry density. During the manual compaction process, in particular, it is not easy to achieve uniform density among the successive layers; the compaction applied on each layer may not be uniform due to unavoidable variation in the manual compaction forces being employed. In addition, compaction of the upper layers would inevitably reduce the thickness of the lower layers. Because the density of the successive layers is unpredictable, the reproducibility of such specimens tends to be inaccurate.

To obtain more uniform density of the specimens, the traditional technique of manual compaction has been replaced in this study by controlling the compaction energy employed. For each specimen, as schematically shown in Fig. 5, a hammer of 12 kg mass was dropped from a fixed height for a fixed number of times. The hammer was lifted using a motor-driven system. This method is herein named as ''automatic compaction''. It enables us to determine the exact compaction energy to be deployed for achieving the required dry density. This process is also easily replicable. Refer to Maqbool and Koseki (2007) for the details of the apparatus for automatic compaction.

In this study, four different compaction energies were employed: i.e., 680, 2700, 6200 and 8685 kJ/m^3. Test conditions are given in Table 2. For each level of compaction energy, two specimens were prepared deploying exactly the same procedures for confirming reproducibility in terms of dry density as shown in Fig. 6. The dry densities obtained were in the range of 1.90–2.17 g/cm^3, while their difference for each compaction level was less than 1%.

Of the above eight specimens, four specimens labeled as TC-1, TC-2, TC-3 and TC-4 were used for conducting monotonic triaxial compression tests. For the cyclic loading triaxial compression tests, two additional specimens labeled as TC-5 and TC-6 were prepared at compaction level of 620 kJ/m^3. Each specimen measured 50 cm high and 23.5 cm times 23.5 cm in cross-section. It was pre-

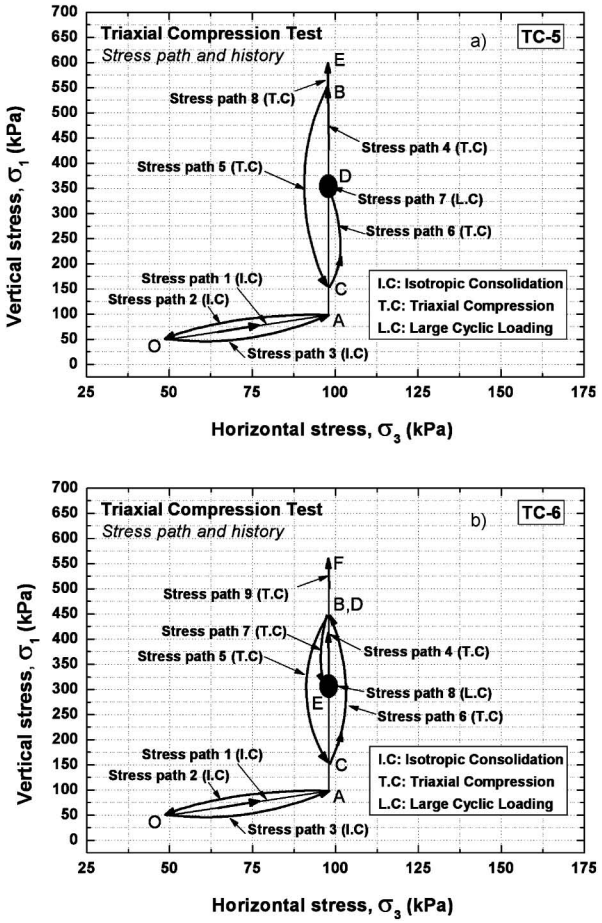

Fig. 4. Stress path in large cyclic loading triaxial compression tests; (a) TC-5 and (b) TC-6

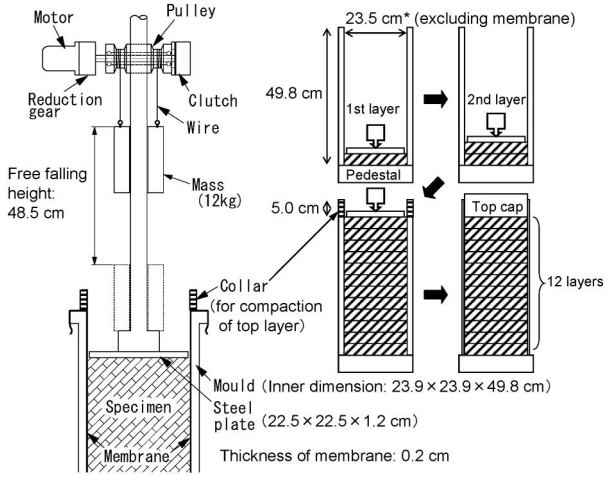

Fig. 5. Schematic diagram of specimen preparation employing automatic compaction (modified after Maqbool and Koseki, 2007)

Table 2. Testing conditions in monotonic and large cyclic triaxial compression tests

Specimen No	Test Code	Testing Condition	No. of Blows per Layer	Fall Height (cm)	Compaction Energy (kJm^3)	Dry Density (g/cm^3)
1	TC–1	Monotonic	33	44	680	1.92
2	TC–2	Monotonic	130	44	2700	2.01
3	TC–3	Monotonic	247	44	5120	2.06
4	TC–4	Monotonic	386	44	8685	2.17
5	TC–5	Large cyclic	30	44	620	1.90
6	TC–6	Large cyclic	30	44	620	1.90

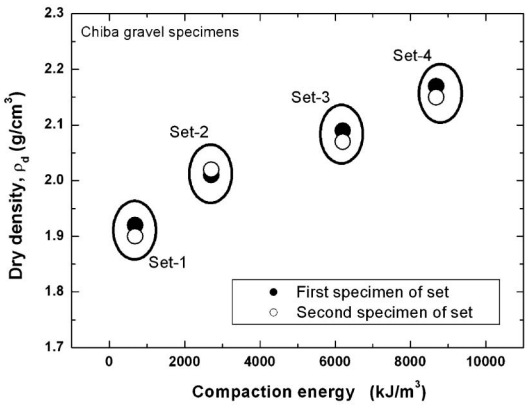

Fig. 6. Reproducibility in terms of dry density of compacted gravel

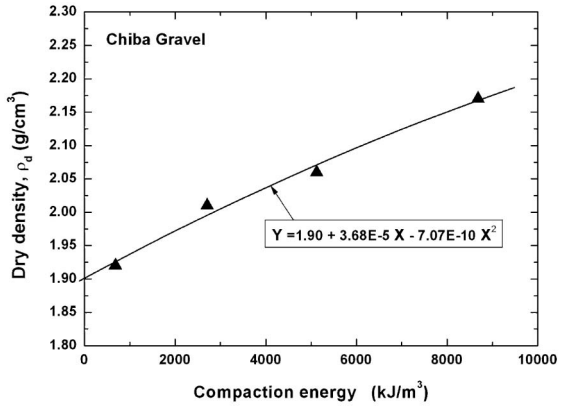

Fig. 7. Relationship between compaction energy and dry density

pared in 12 layers with a compacted thickness of 4.0–4.5 cm per layer. The surface of the preceding layer was scraped in order to ensure good interlocking between successive layers.

Optimum moisture content of the tested gravel was determined from the compaction curves drawn for three levels of compaction energy: 620, 2700 and 7820 kJ/m^3 (Maqbool and Koseki, 2007). It was found that the values of the optimum moisture content were different for each level of compaction. In order to keep consistency in the specimen preparation procedure, the optimum moisture content (=5.5%) obtained for the maximum level of compaction (=7820 kJ/m^3) was employed for all the compaction levels.

As a result of this study, the trend of the curve between compaction energy and dry density was found to be slightly non-linear as shown in Fig. 7. Their relationship is approximated by the equation shown in the figure. The relationship suggests that increase in compaction energy beyond a certain limit would not significantly increase the dry density.

It should be noted that the above evaluation of the linearity or non-linearity in Fig. 7 was made in a subjective manner, since the number of available data was limited to be four. It will be also the case with the relevant figures to be shown in the next section (Figs. 9 through

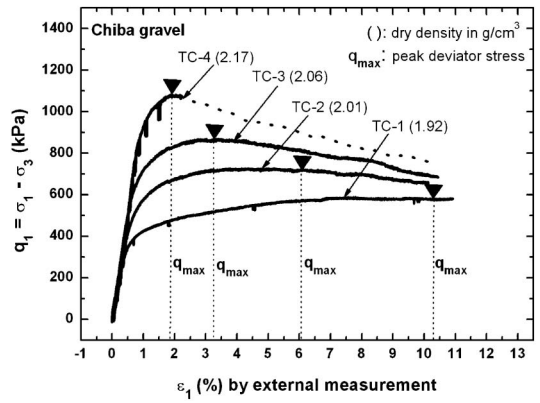

Fig. 8. Externally measured axial strain versus deviator stress for monotonic triaxial compression tests

12). Since the physical meaning of the parameters that are compared in these figures was different from each other, it was not possible for the authors to deduce the essential linearity or non-linearity in an objective manner.

TRIAXIAL TEST RESULTS AND DISCUSSIONS

Monotonically Loaded Triaxial Compression Test Results and Discussion

The relationship between deviator stress ($q_1=\sigma_1-\sigma_3$) and axial strain (ε_1) for all four monotonically loaded triaxial compression (stress path 4 in Fig. 3) tests is shown in Fig. 8. From this relationship, we can compute maximum deviator stress (q_{max}) and peak angle of internal friction (ϕ_{max}) by assuming no cohesion by the following equations;

$$q_{max}=(\sigma_1-\sigma_3)_{max} \quad (1)$$

$$\phi_{max}=\sin^{-1}[(\sigma_1-\sigma_3)/(\sigma_1+\sigma_3)]_{max} \quad (2)$$

In these equations σ_1 is the major principle stress, and σ_3 is the minor principal stress that is equal to the confining stress in this study.

It was observed that the q_1 values corresponding to similar axial strain levels were larger in denser specimens than those in relatively loose specimens. In tests TC-1, TC-2, TC-3 and TC-4, q_{max} was observed at about 10.3%, 6%, 3.3% and 1.9% of axial strain, respectively. Post peak behavior was recorded in the three tests TC-1, TC-2 and TC-3; however, it could not be recorded in test TC-4 because the loading was stopped just after reaching q_{max} due to mechanical dysfunction of the hydraulic pump. The expected post peak behavior of test TC-4 is indicated by dotted line in Fig. 8.

The relationship between q_{max} and compaction energy was found to be non-linear; the slope of the curve becoming milder with the increase in compaction energy as approximated by the equation shown in Fig. 9. On the other hand, the relationship between q_{max} values and dry density was rather linear as plotted in Fig. 10. The practical implication is that there will be an optimum condition for the compaction level beyond which its execution becomes less economical. The relationship between ϕ_{max} values

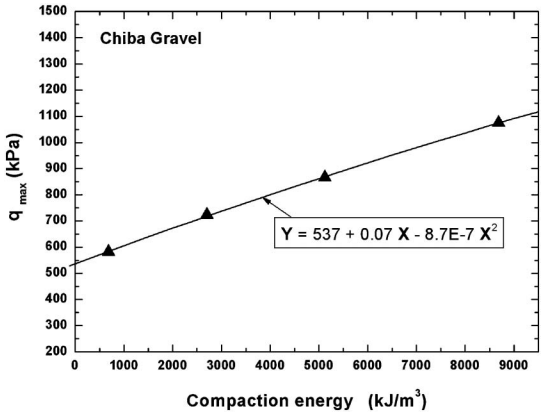

Fig. 9. Relationship between compaction energy and maximum deviator stress

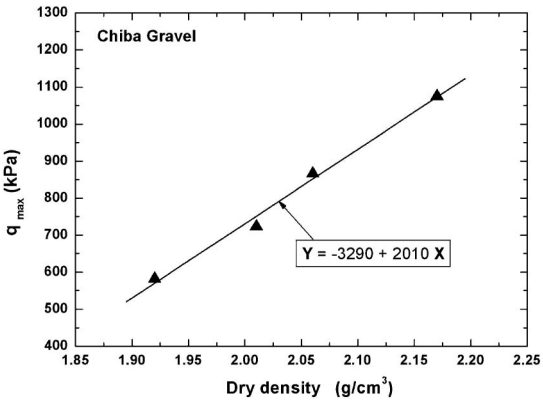

Fig. 10. Relationship between dry density and maximum deviator stress

(obtained from Eq. (2)) with compaction energy was also non-linear; however, the relationship became more linear again with dry density as shown in Figs. 11 and 12.

Dilatancy properties of all four specimens were compared based on their relationship between axial strain (ε_1) and nominal volumetric strain (ε_{vol}); computed by the following equation.

$$\varepsilon_{vol} = \varepsilon_1 + 2 \times \varepsilon_3 \quad (3)$$

Here ε_1 is the axial strain measured externally and ε_3 is the strain measured by C-LDTs. The data obtained by H-LDTs was not used in this computation because of limited range of H-LDTs as compared to C-LDTs.

The values of ε_{vol} in tests TC-1, TC-2 and TC-3 were found similar to each other up to about 3% of ε_1 as shown in Fig. 13. Beyond this range of ε_1, the specimen in test TC-1 prepared by employing lowest compaction energy showed relatively less dilative behaviour than the specimens in tests TC-2 and TC-3. On the other hand the specimen in test TC-4, prepared with the highest compaction energy exhibited largest dilative behaviour than the other three specimens. Such difference in dilatancy curves represented the difference in compaction level and dry density for all four specimens. Since the particles of the tested material were angular, the denser the specimen is, the more likely it is to dilate due to the particles trying to override one another.

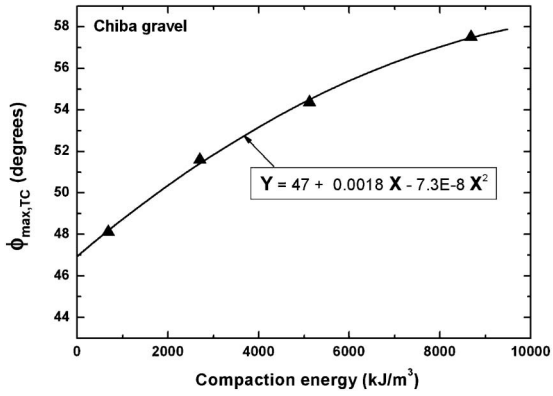

Fig. 11. Relationship between compaction energy and maximum angle of internal friction

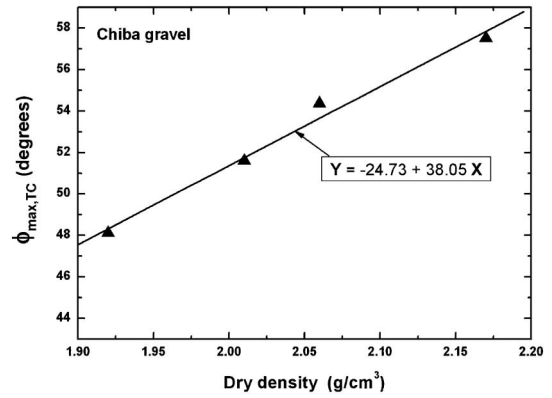

Fig. 12. Relationship between dry density and maximum angle of internal friction

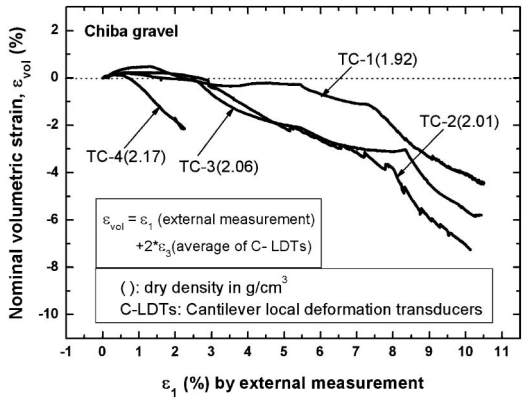

Fig. 13. Externally measured axial strain versus nominal volumetric strain in monotonic triaxial compression tests

Large Cyclic Loading Triaxial Compression Test Results and Discussion

The relationships between deviator stress ($q_1 = \sigma_1 - \sigma_3$) and axial strain ($\varepsilon_1$) for two cyclic loading tests (TC-5 and TC-6) and one monotonically loaded triaxial compres-

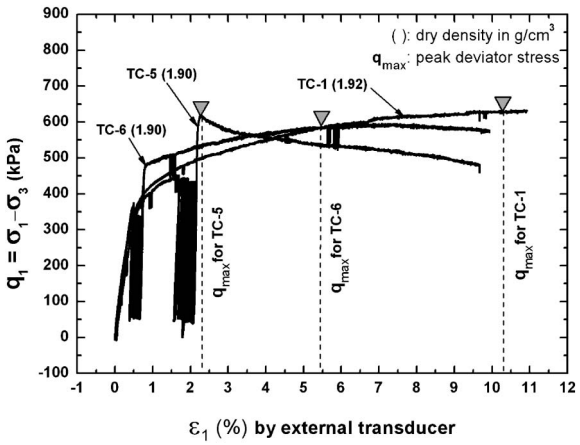

Fig. 14. Externally measured axial strain versus deviator stress (q_1) for test TC-1 and large cyclic loading tests

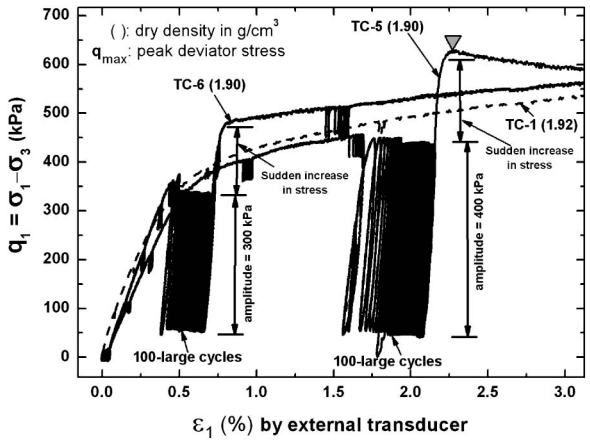

Fig. 15. Externally measured axial strain versus deviator stress (q_1) for test TC-1 and large cyclic loading tests (until axial strains of about 3%)

sion test (TC-1) are shown in Fig. 14. The dry density is similar in all three tests. The only difference among three tests is application of cyclic loading at certain stress level during triaxial compression testing as given in Table 1.

Although the number of tested specimens is limited to three, as can be seen from Fig. 14, the peak strength in these tests was similar to each other irrespective of the difference in the loading histories with/without large cyclic loading. This may suggest that there exists a common limit of stress state beyond which the local soil particle structure starts to fail, triggering overall strain softening behavior. However, as will be compared more in detail later, the values of axial strain at the peak stress state were different among the three tests.

In the first cyclic loading test labeled as TC-5, from a neutral stress state at a deviator stress q_1 of about 245 kPa, 100 cycles of loading/unloading with single amplitude vertical stress of 200 kPa and a frequency of 0.001 Hz were applied. As shown in Fig. 15, during monotonic loading stage after the large cyclic loading, sudden increase in q_1 value without any considerable increase in axial strain was observed. In this test, the peak stress state was obtained immediately after the large cyclic loading at an axial strain of about 2.3%.

In the second cyclic loading test labeled as TC-6, 100 cycles of loading/unloading with single amplitude vertical stress of 150 kPa and a frequency of 0.001 Hz were applied from a neutral stress state at a deviator stress q_1 of 196 kPa. Similar to the first test, as shown in Fig. 15, during monotonic loading stage after the large cyclic loading, sudden increase in q_1 value without any considerable increase in axial strain was observed. On the other hand, q_{max} was observed at larger axial strain, i.e., about 5.5%.

In these tests, during cyclic loading stage, the accumulation of axial strain was larger in the initial cycles and decreased with the increase in number of cycles as shown in Figs. 16 and 17. Moreover, the axial strain increment was larger in test TC-5 due possibly to larger amplitude of cyclic loading than that in test TC-6 as shown in Fig. 18. The unexpected behavior in test TC-5 as shown in Fig. 18

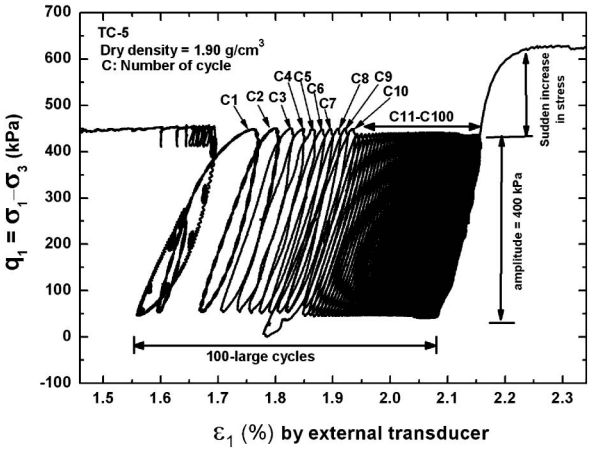

Fig. 16. Externally measured axial strain versus deviator stress (q_1) during large cyclic loading for test TC-5

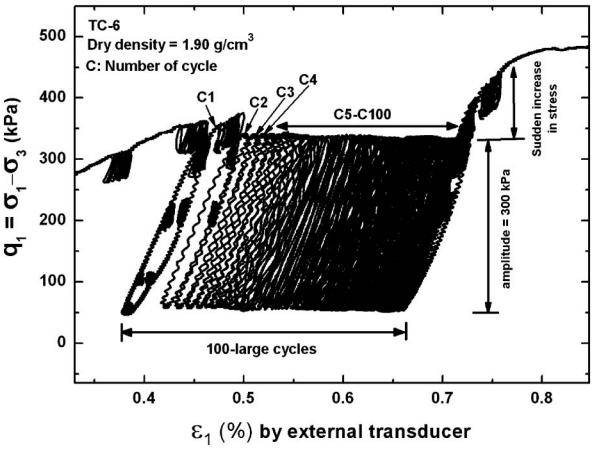

Fig. 17. Externally measured axial strain versus deviator stress (q_1) during large cyclic loading for test TC-6

was due to mechanical problem in the loading control which was immediately repaired. It should be noted that creep deformation during large cyclic loading may have

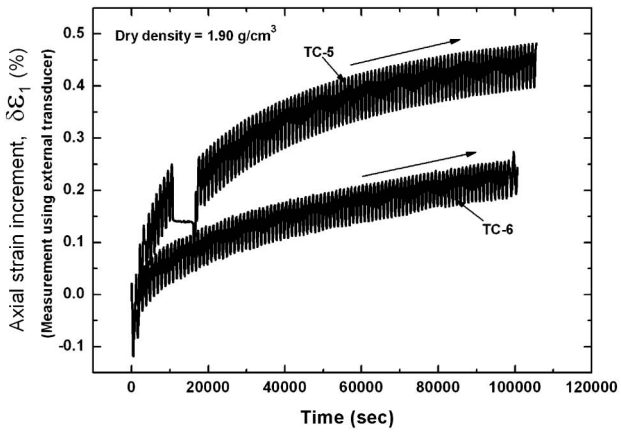

Fig. 18. Time versus axial strain increment during large cyclic loading in tests TC-5 and TC-6

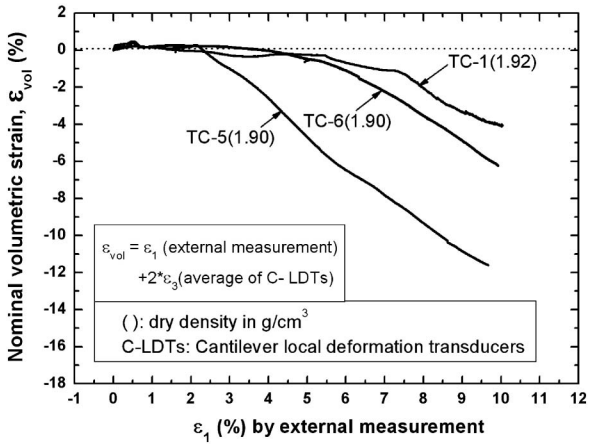

Fig. 20. Externally measured axial strain versus nominal volumetric strain in monotonic (TC-1) and large cyclic loading tests

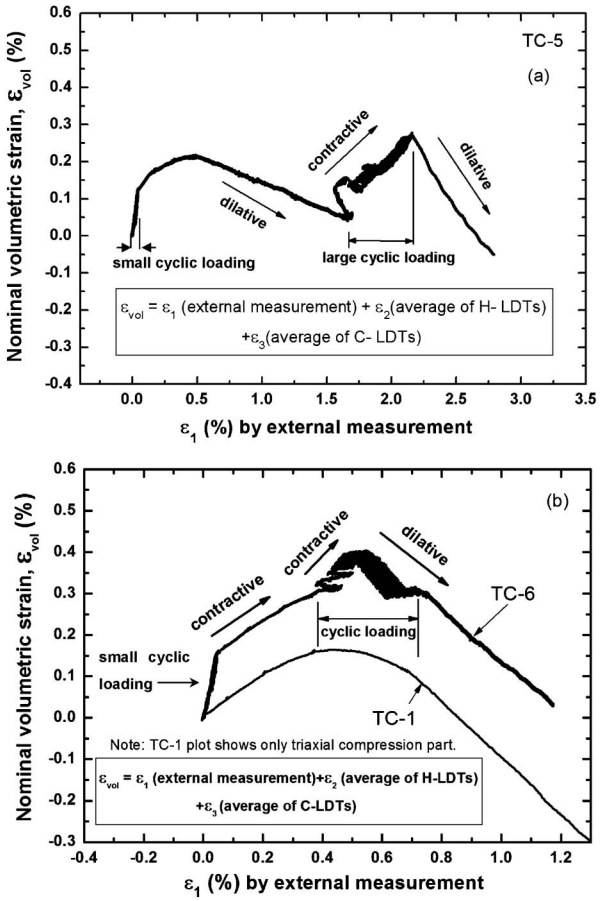

Fig. 19. Externally measured axial strain versus nominal volumetric strain in large cyclic loading tests: (a) TC-5 and (b) TC-6

affected the above behavior as well, since the maximum stress levels mobilized were relatively high (i.e., about 60–70% of the peak stress levels).

As shown in Fig. 19(a), the measured volumetric strain during large cyclic loading in test TC-5 exhibited contractive behavior, suggesting improvement of soil fabric by re-arrangement of particles. This re-arrangement of particles during cyclic loading may have caused earlier dilative behaviour in test TC-5 than the other two specimens as shown in Fig. 20, which also resulted into earlier mobilization of the peak stress state as mentioned before (Fig. 14).

On the other hand, in test TC-6 (Fig. 19(b)), the specimen response during large cyclic loading changed from contractive to dilative behavior. During the subsequent monotonic loading, it exhibited dilative behavior that was similar to the behavior observed in the monotonic loading test (test TC-1) as plotted on the same figure. Such different trends of dilatancy behavior during large cyclic loading between the two tests (tests TC-5 and TC-6) may be linked to the different axial strain levels that were mobilized at the peak stress state, as mentioned previously. Further studies are required on the effects of cyclic loading amplitudes on the possible change in the soil fabric.

It should be noted that the effect of large cyclic loading on small strain stiffness of compacted gravel has been studied and reported by AnhDan and Koseki (2004). Therefore, its effect on the peak strength and dilatancy characteristics is focused in this section. On the other hand, in the next section, the effect of different compaction energies on small strain stiffness of compacted gravel without the large cyclic loading history will be studied.

Effect of Compaction Energy on Small Strain Stiffness

To study the effect of compaction energy on small strain stiffness of compacted gravel, vertical Young's moduli were measured by employing static and dynamic techniques. To evaluate quasi-elastic vertical Young's moduli based on static measurement (E_s), existing data on the deformation properties from cyclic loading tests on dense gravelly soils reported in the literature showed that the behavior at strains lesser than about 0.001% is nearly elastic (Kokusho and Esashi, 1981, Jiang et al., 1997). In our study, the specimen was subjected to very small unloading/reloading cycles at specific stress levels in the vertical direction. For each stress level, stress-strain relationship during small vertical loading cycle is depicted

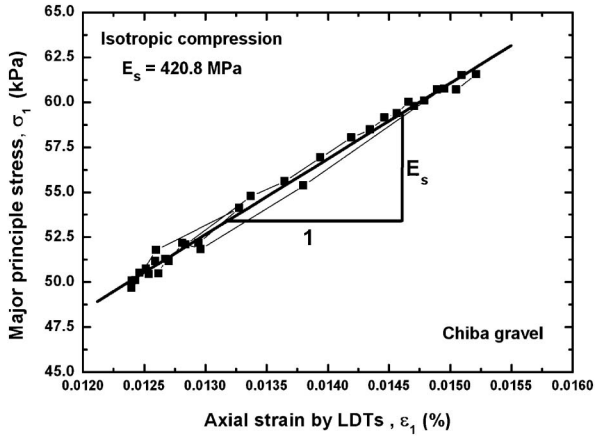

Fig. 21. Typical stress-strain relationship during a small vertical loading cycle

by a straight line, and E_s is evaluated from the slope of the line. Typical stress-strain relationship during a small vertical loading cycle is shown in Fig. 21.

For dynamic measurements, in order to receive a clear signal, AnhDan et al. (2002) employed continuous sinusoidal inputs for trigger excitation while testing on gravel specimens by using the same equipment as used in this study. In their approach, it was sometimes difficult to detect the correct set of corresponding peak signals measured at different levels. Moreover, they neglected to consider the effects of reflected waves for travel time determination. In the present study, therefore, a different approach was devised to determine accurately the wave travel time. Single pulse wave at specific stress levels was generated using a trigger that was set on the top cap, and the wave travel time was determined using two accelerometers that were attached on the side of specimen as shown in Photo 2. In this approach, by considering the first peak point in computing the wave travel time, the problem of reflected wave arrival could be eliminated. Finally, from the obtained wave travel time, the wave velocity was evaluated. As the top cap touched the whole cross-section of the specimen that was with free side boundaries, we assumed that unconstrained compression waves were measured at the side of the specimen where the accelerometers were attached. Its wave velocity V_p is directly related to E_d of the material as given in the following equation:

$$E_d = \rho V_p^2 \tag{4}$$

where ρ is the mass density of the specimen, and V_p is the compression wave velocity. The latter was calculated by the equation:

$$V_p = L/t \tag{5}$$

where L is the distance covered by the wave as defined in Photo 2 and t is the wave travel time.

To determine the wave travel time (t), it was decided to use the first peaks of the waves (Fig. 22) that were measured at different levels after a detailed study given in Maqbool (2005). It should be noted that the E_d values can be alternatively evaluated under an assumption of constrained condition and isotropic deformation properties by using the following equation. Refer to AnhDan et al. (2002) for more detailed discussion considering anisotropic deformation properties.

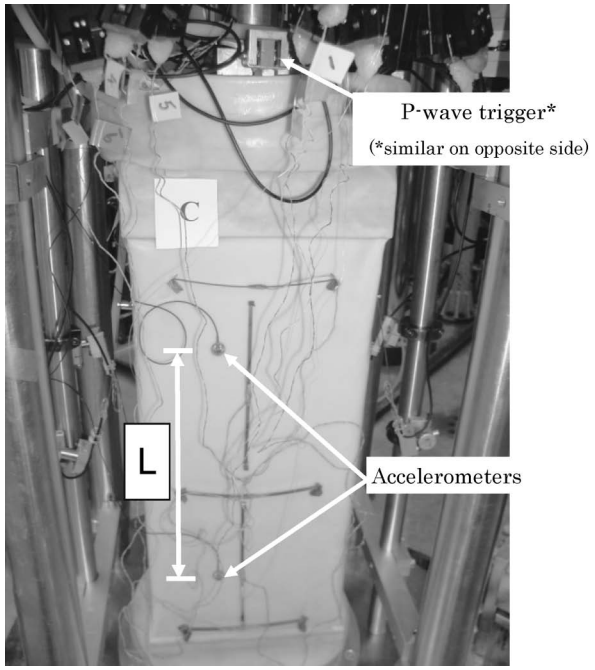

Photo 2. P-wave triggers and accelerometers set on large scale prismatic specimen of gravel

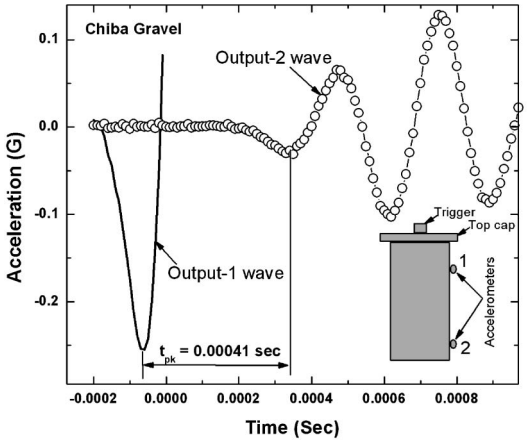

Fig. 22. Typical wave record to measure wave travel time

$$M = \rho V_c^2 = \frac{E_d(1-\nu)}{(1-2\nu)(1+\nu)} \tag{6}$$

where M is the constrained modulus, V_c is the compression wave velocity under constrained condition and ν is the Poisson's ratio.

The values of the small strain Poisson's ratio under isotropic stress states were found to be around 0.18–0.20 in this study. With these values of Poisson's ratio, the above E_d values under an assumption of constrained condition will be around 8–11% larger than the E_d values employed in this study under an assumption of uncon-

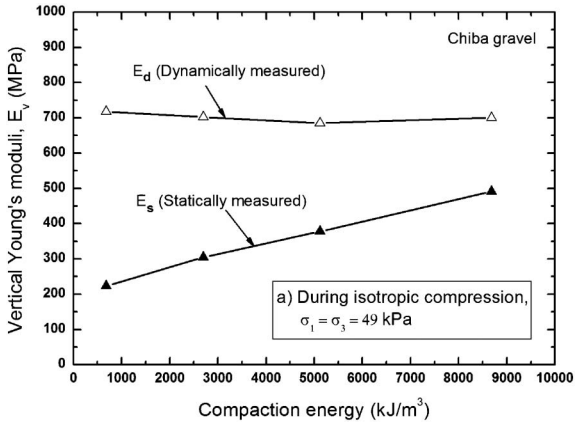

(a) at isotropic stress state of 49 kPa

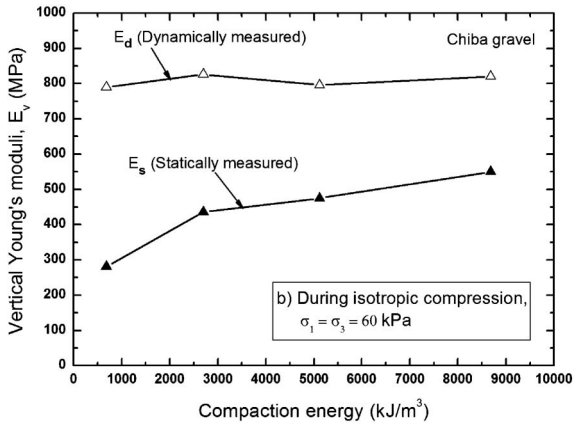

(b) at isotropic stress state of 60 kPa

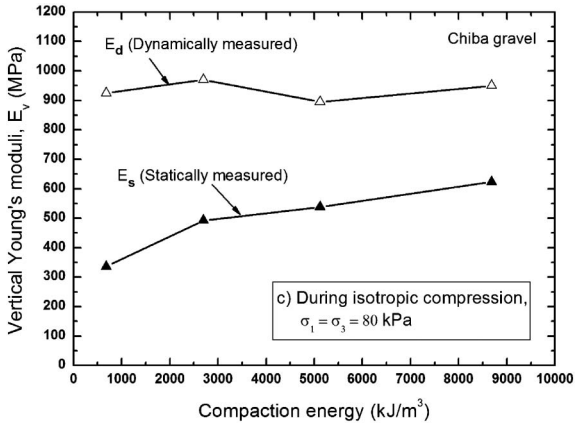

(c) at isotropic stress state of 80 kPa

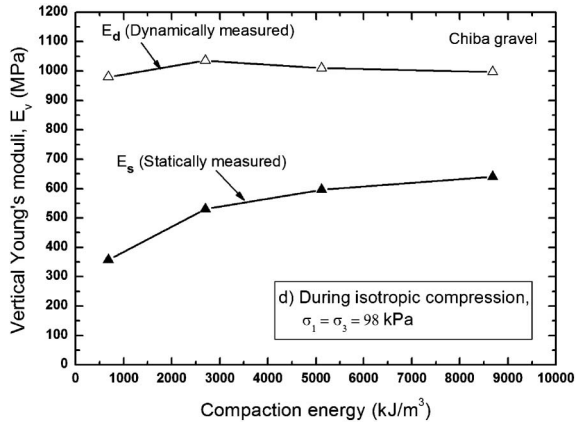

(d) at isotropic stress state of 98 kPa

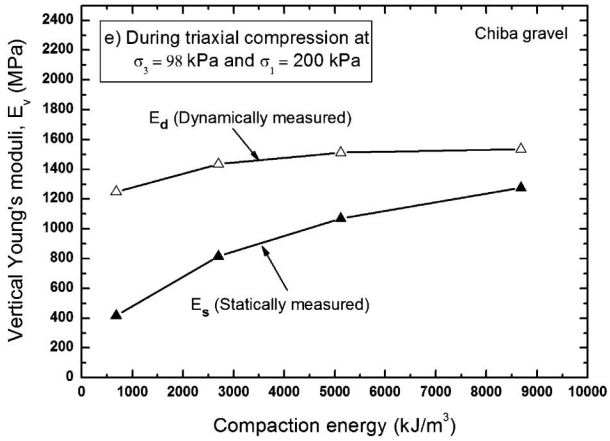

(e) at anisotropic stress state of $\sigma_3 = 98$ kPa and $\sigma_1 = 200$ kPa

Fig. 23. Relationship between compaction energy and vertical Young's moduli in tests TC-1 through TC-4

strained condition.

Note also that the frequencies of the single pulse wave employed in this study were in a range of 3.0 to 5.0 kHz. They correspond to wave lengths λ of 0.097 to 0.264 cm, considering that the wave velocities measured in this study were 404 to 734 m/sec. When they are normalized with the height of the specimen, H (= 50 cm) and the mean diameter of the tested material, d_{50} (= 6.0 cm), the ratios of λ/H and λ/d_{50} are 1/500 to 1/200 and 1/60 to 1/20, respectively. Since the λ values are much smaller than the equivalent radius of the specimen, r_{eq} (= 13.3 cm), which is evaluated by Eq. (7) assuming an equivalent cylinder having the same cross-sectional area, the assumption of rod wave (i.e., for a condition of $\lambda \gg r_{eq}$, according to Santamarina, 2001) would not be relevant in this study.

$$r_{eq} = \sqrt{\frac{L \cdot W}{\pi}} \tag{7}$$

where L and W are the horizontal dimensions of the prismatic specimen (refer to Fig. 1).

Figure 23 compares the E_s and E_d values that were evaluated at several stress states during isotropic compression and triaxial shearing. With the increase in compaction energy, the E_s values increased. On the other hand, E_d values did not increase but were maintained almost constant.

The present study could reveal that at the same compaction level, the E_d value was larger than the E_s value, while their difference was reduced as a result of increase in compaction energy or dry density; thus indicating the need for developing a proper ''correction factor'' for

measuring small strain stiffness of compacted gravel, which would depend on the levels of compaction energy or dry density and the conditions of dynamic measurement if it is employed.

The reason for the above behavior might be that in the dynamic measurement, unlike the static measurement, the wave does not reflect the overall cross-sectional property of the specimen; rather it travels through the shortest path made by the interlocking of bigger particles resulting in larger values of Young's moduli (Tanaka et al., 2000; AnhDan and Koseki, 2002). The difference in the two Young's moduli would increase with the decrease in the dry density. Since looser specimens would have larger structural or microscopic heterogeneity than denser ones, the static measurement results would be affected directly by it. On the other hand, the dynamic measurement results were not affected largely, because certain amounts of compaction were applied to all the specimens during preparation process and possibly created interlocking of bigger particles.

CONCLUSIONS

This study revealed the following conclusions;

1) The automatic compaction technique makes it possible to obtain highly dense specimens as well as to evaluate compaction energy. The trend of the curve between compaction energy and dry density is found to be slightly non-linear, which suggests that increase in compaction energy beyond a certain limit would not result in further significant increase in dry density.
2) The peak strength of compacted gravel increases in a non-linear manner with the increase in compaction energy, and the slope of the curve becomes milder; therefore, there will be an optimum condition for the compaction level beyond which its execution in practice would be less economical.
3) There exists difference between statically and dynamically measured small strain Young's moduli of compacted gravel. They narrow as a result of increase in compaction energy; thus indicating the need for developing a proper ''correction factor'' for evaluating small strain stiffness of compacted gravel.
4) The peak strength in three almost equally dense specimens was found to be similar irrespective of the difference in the loading histories with/without large cyclic loading. On the other hand, the values of axial strain at the peak stress state were different among the three tests. Moreover, during monotonic loading stage just after the large cyclic loading, sudden increase in the shear stress level without any considerable increase in axial strain was observed. Such behavior may be affected by possible re-arrangement of particles during the large cyclic loading.

ACKNOWLEDGEMENTS

The authors express their sincere thanks to the Ministry of Science, Culture and Education of Japan for its financial support to the first author for his PhD studies at the University of Tokyo, Japan. They also thank Mr. Takeshi Sato, formerly Research Support Promotion Member, Institute of Industrial Science, the University of Tokyo, Japan for providing technical support in conducting the laboratory tests.

NOTATIONS

ε_1: Axial strain
ε_3: Lateral strain
ε_{vol}: Nominal volumetric strain
σ_1: Axial stress
σ_3: Lateral confining stress
U_c: Uniformity coefficient
G_s: Specific gravity
q_{max}: Maximum deviator stress
ϕ_{max}: Peak angle of internal friction
ASTM: American Society for Testing and Materials
LDTs: Local Deformation Transducers
H-LDTs: Horizontal Local Deformation Transducers
C-LDTs: Cantilever Local Deformation Transducers
I.C.: Isotropic Consolidation
V_p: Compression wave velocity
E_d: Small strain vertical Young's modulus by dynamic measurement
ρ: Mass density of the specimen
L: Distance covered by wave
t: Wave travel time
M: Constrained modulus
V_c: Compression wave velocity under constrained condition
E_s: Vertical Young's modulus obtained by static measurement
ν: Poisson's ratio

REFERENCES

1) AnhDan, L. Q., Koseki, J. and Sato, T. (2002): Comparison of Young's moduli of dense sand and gravel measured by dynamic and static methods, *Geotechnical Testing Journal*, ASTM, **25**(4), 349–368.
2) AnhDan, L. Q. and Koseki, J. (2004): Effects of large number of cyclic loading on deformation characteristics of dense granular materials, *Soils and Foundations*, **44**(3), 115–123.
3) AnhDan, L. Q., Koseki, J. and Sato, T. (2006a): Evaluation of quasi-elastic properties of gravel using a large scale true triaxial apparatus, *Geotechnical Testing Journal*, ASTM, **29**(5), 374–384.
4) AnhDan, L. Q., Tatsuoka, F. and Koseki, J. (2006b): Viscous effects on the stress-strain behavior of gravelly soil in drained triaxial compression, *Geotechnical Testing Journal*, ASTM, **29**(4), 330–340.
5) Balakrishnaiyer, K., Koseki, J., Modoni, G., AnhDan, L. Q. and Tatsuoka, F. (1998): Deformation characteristics at small strain levels of dense gravel, *Geotechnics of Hard Soils and Soft Rocks*, eds. by Evangelista and Picarelli, Balkema, **1**, 423–430.
6) Burmister, D. M. (1964): Environmental factors in soil compaction, *Compaction of Soils*, ASTM special technical publication (377), 47–66.
7) Dong, J. and Nakamura, K. (1997): Anisotropic deformation and strength characteristics of gravels in large-scale plane strain and triaxial compression tests, *Proc. 14th International Conference on Soil Mechanics and Foundation Engineering*, Hamburg, 81–84.

8) Goto, S., Tatsuoka, F., Shibuya, S., Kim, Y. S. and Sato, T. (1991): A simple gauge for local small strain measurements in the laboratory, *Soils and Foundations*, **31**(1), 169–180.
9) Hayano, K., Koseki, J., Sato, T. and Tatsuoka, F. (1999): Small strain deformation characteristics of sedimentary soft mudstone from true triaxial tests, *Pre-failure Deformation Characteristics of Geomaterials*, eds. by Jamiolkowski, Lancellotta and Lo Presti, **1**, 191–198.
10) Holtz, W. G. and Gibbs, H. J. (1956): Triaxial shear tests on pervious gravelly soils, *Journal of Soil Mechanics and Foundation Division*, Proc. of ASCE, **82**(SM1), 1–22.
11) Holtz, W. G. and Ellis, W. (1963): Comparison of the shear strengths of laboratory- and field-compacted soils, *Laboratory Shear Testing of Soils*, ASTM special technical publication (361), 471–480.
12) Jiang, G. L., Tatsuoka, F., Flora, A. and Koseki, J. (1997): Inherent and stress-state-induced anisotropy in very small strain stiffness of a sandy gravel, *Geotechnique*, **47**(3), 509–521.
13) Kohata, Y., Jiang, G. L., Murata, O. and Tatsuoka, F. (1999): Elastic-properties-based modeling of non-linear deformation characteristics of gravels, *Pre-failure Deformation Characteristics of Geomaterials*, eds. by Jamiolkowski, Lancellotta and Lo Presti, **1**, 533–539.
14) Kokusho, T. and Esashi, Y. (1981): Cyclic triaxial tests on sands and coarse materials, *Proc. 10th International Conference on Soil Mechanics and Foundation Engineering*, Stockholm, **1**, 673–676.
15) Koseki, J., Tateyama, M., Watanabe, K. and Nakajima, S. (2007): Stability of earth structures against high seismic loads, Keynote Lecture, *Proc. 13th Asian Regional Conference on Soil Mechanics and Geotechnical Engineering*, Kolkata, **2**, 222–241.
16) Maqbool, S. (2005): Effect of compaction on strength and deformation properties of gravel in triaxial and plane strain compression tests, *PhD thesis*, Department of Civil Engineering, The University of Tokyo, Japan.
17) Maqbool, S. and Koseki, J. (2007): Large-scale plane strain compression tests on compacted gravel with active and passive controls, *Soils and Foundations*, **47**(6), 1063–1073.
18) Marachi, N. D., Chan, C. K., Seed, H. B. and Duncan, J. M. (1969): Strength and deformation characteristics of rockfill materials, Report No. TE-69-5, Department of Civil Engineering, University of California, Berkeley, 139.
19) Marachi, N. D., Chan, C. K. and Seed, H. B. (1972): Evaluation of properties of rockfill materials, *Journal of Soil Mechanics and Foundation Division*, Proc. of ASCE, **98**(SM1), 95–114.
20) Marsal, R. (1967): Large scale testing of rockfill materials, *Journal of Soil Mechanics and Foundation Division*, Proc. of ASCE, **93**(SM2), 27–43.
21) Massarsch, K. R. and Fellenius, B. H. (2002): Vibratory compaction of coarse-grained soils, *Canadian Geotechnical Journal*, **39**(3), 695–709.
22) Okuyama Y., Yoshida, T., Tatsuoka, F., Koseki, J., Uchimura, T., Sato, N. and Oie, M. (2003): Shear banding characteristics of granular materials and particle size effects on the seismic stability of earth structures, *Deformation Characteristics of Geomaterials*, eds. by Di Benedetto, Doanh, Geoffroy and Sauzeat, **1**, 607–616.
23) Santamarina, J. C. (2001): *Soils and Waves*, John Wiley & Sons, Ltd., 194–195.
24) Tanaka, Y., Kudo, K., Nishi, K., Okamoto, T., Kataoka, T. and Ueshima, T. (2000): Small strain characteristics of soils in Hualien, Taiwan, *Soils and Foundations*, **40**(3), 111–125.
25) Tatsuoka, F., Yamada, K., Yasuda, M., Yamada, S. and Manabe, S., (1991): Cyclic undrained behavior of an undisturbed gravel for aseismic design of a bridge foundation, *Proc. 2nd International Conference on Recent Advances in Geotechnical Earthquake Engineering and Soil Dynamics*, St. Louis, **1**, 141–148.
26) Tatsuoka, F. and Shibuya, S. (1992): Deformation characteristics of soils and rocks from field and laboratory tests, *Proc. 9th Asian Regional Conference of Soil Mechanics and Foundation Engineering*, Bangkok, **2**, 101–170.
27) Tatsuoka, F. and Kohata, Y. (1995): Stiffness of hard soils and soft rocks in engineering applications, *Pre-failure Deformation of Geomaterials*, eds. by Shibuya, Mitachi and Miura, **2**, 947–1066.
28) Yasuda, N. and Matsumoto, N. (1994): Comparisons of deformation characteristics of rockfill materials using monotonic and cyclic loading laboratory tests and in situ tests, *Canadian Geotechnical Journal*, **31**(3), 162–174.